The following publication H. Zhang, C. Fu, Y. Chan, S. Tsang and W. Siu, "Probability-Based Depth Intra-Mode Skipping Strategy and Novel VSO Metric for DMM Decision in 3D-HEVC," in IEEE Transactions on Circuits and Systems for Video Technology, vol. 28, no. 2, pp. 513-527, Feb. 2018 is available at https://doi.org/10.1109/TCSVT.2016.2612693.

Probability-based Depth Intra Mode Skipping Strategy and Novel VSO Metric for DMM Decision in 3D-HEVC

Hong-Bin Zhang, Chang-Hong Fu, *Member, IEEE*, Yui-Lam Chan, *Member, IEEE*, Sik-Ho Tsang, *Member, IEEE*, and Wan-Chi Siu, *Fellow, IEEE*

***Abstract*— Multi-view video plus depth (MVD) format has been adopted as the emerging 3D video representation recently. It includes a limited number of textures and depth maps to synthesize additional virtual views. Since the quality of depth maps influences the view synthesis process, their sharp edges should be well preserved to avoid mixing foreground with background. To address this issue, 3D-HEVC introduces new coding tools, a partition-based intra mode (depth modelling mode, DMM), a residual description technique (segment-wise depth coding, SDC), and a more complex Rate-Distortion (RD) evaluation with view synthesis optimization (VSO), to provide more accurate predictions and achieve higher compression rate. However, these new techniques introduce a lot of possible candidates and each of them requires complicated RD calculation in the process of intra mode decision. They lead to unacceptable computational burden in a 3D-HEVC encoder. Therefore, in this paper, we raise two efficient techniques for depth intra mode decision. First, by investigating the statistical characteristics of variance distributions in the two partitions of DMM, a simple but efficient criterion based on the squared Euclidean distance of variances (SEDV) is suggested to evaluate RD costs of the DMM candidates instead of the time-consuming VSO process. Second, a probability-based early depth intra mode decision (PBED) is proposed to select only the most promising mode and make the early determination of using SDC based on the low complexity RD-Cost in rough mode decision. Experimental results show that the proposed algorithm with these two new techniques provides 33%-48% time reduction with little drops of the coding performance compared with the state-of-the-art algorithms.**

***Index Terms*—3D-HEVC, depth map, depth modelling mode, fast algorithm, multi-view video plus depth, intra coding, rough mode decision.**

I. Introduction

In the last few years, 3D videos have attracted more and more attention from the academia and industry after a great achievement in the film industry. Pervasive applications include immersive video conference developed by Heinrich Hertz Institute (HHI) [1], 3D movie, Microsoft motion sensing game (XBOX) [2], etc. In principle, 3D scene perception can be achieved by presenting two different videos to the viewer's left and right eyes simultaneously [3]. Owing to limitations in the production environment and bandwidth constraints [4], only limited views and their corresponding depth maps are captured, compressed and transmitted for 3D video applications [5]-[6], and this 3D video format is referred to as multi-view video plus depth (MVD) [7]. With the aid of depth information, it can synthesize an arbitrary number of views from these limited views via the depth-image-based rendering (DIBR) technology [8] at decoder side. This new MVD has been adopted by the state-of-the-art High Efficiency Video Coding (HEVC) standard [9]. Recently, the Joint Collaborative Team on 3D Video Coding Extension (JCT-3V) has been developing a new generation of an international 3D video coding standard - 3D-HEVC [10].

In MVD, depth samples describe the distance between a camera and an actual object as a gray-level image. The characteristics of depth maps are quite different from texture images. Firstly, the depth maps have mostly smooth regions delimited by sharp edges [7]. Secondly, the distortion of sharp edges induces ringing artifacts at object boundaries in synthesized views [11]. Finally, depth maps are transmitted for view synthesis instead of directly viewed by audiences. Unlike 2D video, preserving the sharp edges rather than the visual quality becomes the most critical task for depth map coding in 3D-HEVC. Consequently, the investigation into alternative depth map coding tools has been carried out. The new tools include depth modelling mode (DMM) [12], segment-wise depth coding (SDC) [13] and view synthesis optimization (VSO) [12], which are designed to preserve the sharp edges in the coded depth maps. DMM is a new intra mode of depth maps in 3D-HEVC, which allows non-rectangle partitions, namely wedgelet [14] and contour [15]. DMM provides a great flexibility to represent the sharp edge, produces accurate predictions, and indicates the edge information efficiently. It can save about 5% of the transmitted bitrate for the same synthesized view quality [16]-[17]. SDC is an alternative coding path to represent the residual signal by a constant pixel value (CPV) instead of the conventional transformed and quantization coefficients. VSO is a complex Rate Distortion

Maiuscript received xxxx, xxxx; revised xxxx, xxxx; accepted xxxx, xxxx. This work is supported in part by National Natural Science Foundation of China (No. 61301109), and a grant from the Research Grants Council of the HKSAR, China (Grant No. PolyU 512016/14E)

H. -B. Zhang and C. -H. Fu are with the School of Electronic and Optical Engineering, Nanjing University of Science and Technology, Nanjing, 210019 CHINA. (e-mail: hongbinzhang0801@sina.cn; enchfu@njust.edu.cn).

Y. -L. Chan, S. -H. Tsang and W. -C. Siu are with the Centre for Signal Processing, the Hong Kong Polytechnic University, Hong Kong (e-mail: enylchan@polyu.edu.hk; en.ho@connect.polyu.hk; enwcsiu@polyu.edu.hk).

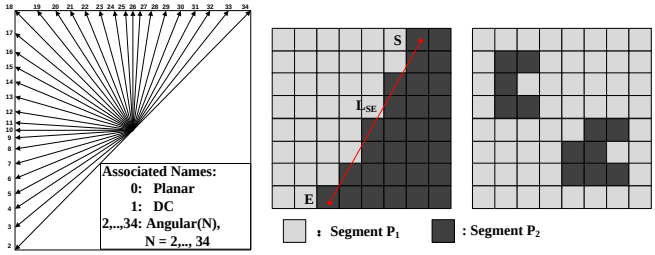

(a) (b) (c)

Fig. 1. Depth intra modes in 3D-HEVC, (a) 35 HEVC traditional intra modes, (b) DMM1, and (c) DMM4.

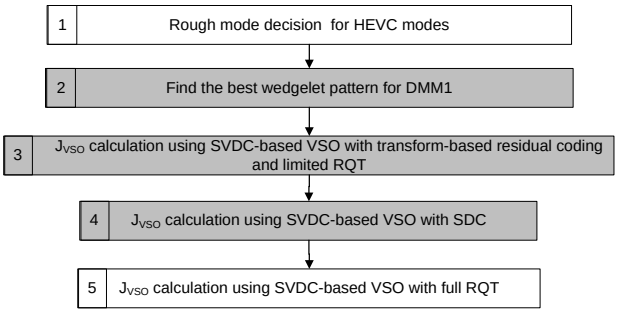

Fig. 2. Depth intra mode decision for an N×N prediction unit.

Optimization (RDO), measuring the synthesized view distortion, to determine the best modes and coding unit partition. Besides, the well-known complex quadtree coding structure of HEVC [18] is also used in 3D-HEVC. Hence, the encoder needs to check all combinations of block sizes with the additional DMM with and without SDC by the complex VSO evaluation. These new coding tools improve the coding efficiency significantly at the expense of high computational complexity cost. Hence, a more efficient depth intra coding process of 3D-HEVC is highly demanded for practical applications.

The organization of this paper is as follows. In Section II, we review the new coding tools for depth intra prediction and its complexity. Then, related works are summarized in Section III. A simple but efficient VSO metric for DMM decision is described in Section IV. Meanwhile, a probability-based early depth intra mode decision (PBED) by exploiting the relationship between the low complexity RD-Cost and the final optimal intra prediction mode is given in Section IV. The framework with the two proposed techniques for reducing the complexity of 3D-HEVC is presented. Simulation results are shown and discussed in Section V. Some concluding remarks are provided in Section VI.

II. Depth Coding Tools in 3D-HEVC and Its Complexity

The introduction of depth maps gives a new perspective for video coding and some new intra prediction techniques are custom designed for coding depth maps. In this section, the depth intra mode decision with several new intra prediction coding tools in 3D-HEVC are briefly introduced.

A. View Synthesis Optimization

Since the reconstructed depth map quality cannot guarantee the synthesized view quality, a view synthesis optimization (VSO) scheme is adopted to select the best mode in depth map coding by considering both of the synthesized view and depth map quality. The distortion measure, D_{VSO}, contains the distortion of the synthesized view, D_{syn}, and the distortion of the depth map, D_{dep}, which can be formulated as

$$D_{VSO} = (w_{syn} \times D_{syn} + w_{dep} \times D_{dep}) / (w_{dep} + w_{syn}) \quad (1)$$

where w_{syn} and w_{dep} are the weighting factors of D_{syn} and D_{dep}, respectively. D_{dep} is calculated by the sum of squared error (SSE) or sum of absolute Hadamard transform difference (SATD). The way to compute D_{syn} can be mainly classified into rendering and non-rendering approaches. The complexity demanding rendering approach is known as the synthesized view distortion change (SVDC)-based VSO [19], which directly performs view synthesis using the encoded data and then measure the distortion of the synthesized view D_{syn}. The non-rendering approach is based on the estimated distortion model. The model-based view synthesis distortion (VSD), referred to as VSD-based VSO in [20], weights the depth distortion with the sum of absolute horizontal gradients of the co-located texture as follows

$$VSD = \sum_{(x,y)\in B} \begin{pmatrix} \frac{1}{2} \times \alpha \times \left| S_D(x,y) - S_D'(x,y) \right| \times \\ W_d \times \begin{bmatrix} \left| S_T'(x,y) - S_T'(x+1,y) \right| \\ + \left| S_T'(x,y) - S_T'(x-1,y) \right| \end{bmatrix}^2 \end{pmatrix} \quad (2)$$

where (x,y) is the pixel location in the current block B, S_D and S_D' denote the original and reconstructed depth maps, respectively. S_T' denotes the reconstructed texture. α is the coefficient determined by camera parameters, and W_d is the weighting factor according to the depth distance from the camera. VSD-based VSO estimates D_{syn} without actually performing view synthesis, which can reduce computational complexity with less accuracy as that of SVDC-based VSO.

The computation of the RD-Cost for VSO, J_{VSO}, is then modified as

$$J_{VSO} = D_{VSO} + \lambda \times Rate(Mode) \quad (3)$$

where λ is the Lagrange Multiplier for mode decision, *Mode* is the one of the candidate modes, and *Rate(Mode)* is the rate cost associated with the chosen mode.

B. Depth Intra Mode

Depth map coding in 3D-HEVC consists of 35 traditional intra modes inherited from HEVC [21] as illustrated in Fig. 1(a). The 33 angular intra modes (*Angular*(*i*), *i* is from 2 to 34) can represent different prediction angles. In additional to these angular intra modes, *DC* and *Planar* modes can work well in smooth or nearly constant regions. Two depth modelling modes, DMM1 and DMM4, are further employed in 3D-HEVC to preserve sharp edges of depth maps. DMM1 and DMM4 divide each prediction unit (PU) into two non-rectangle segments and each segment is described by a constant pixel value (CPV). For each wedgelet partition in DMM1, two segments P_1 or P_2 are separated by a straight line L_{SE} as shown in Fig. 1(b). S and E are the start and end points of L_{SE}, respectively. The optimal wedgelet pattern is decided by calculating J_{vso} of all wedgelet

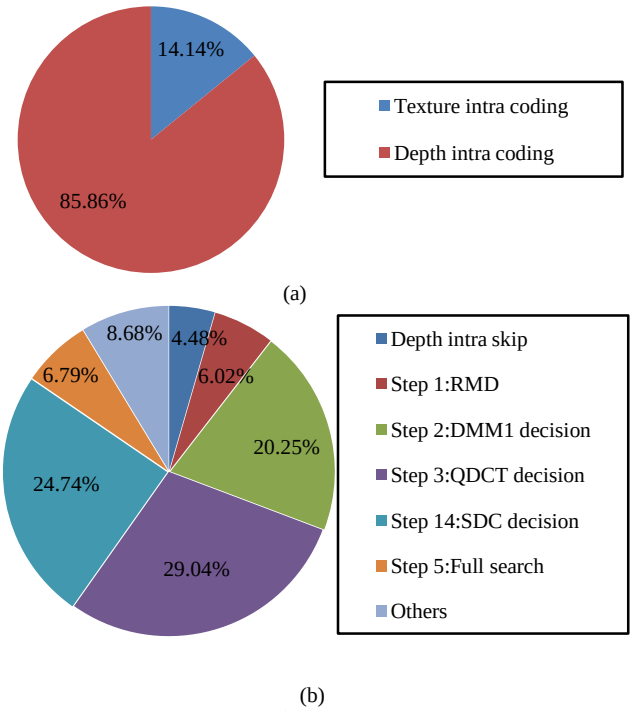

Fig. 3. Encoding time occupation of (a) depth maps and (b) its intra mode decision.

pattern candidates. DMM4 can employ arbitrary contour-partition as shown in Fig. 1(c), which is decided by the co-located reconstructed texture PU with a thresholding method. In the latest test model, HTM-16.0 [22], DMM4 is regarded as an inter-component prediction tool and is no longer used for depth intra slices [23]. Since our paper basically develops fast techniques on intra mode decision, DMM1 is the sole DMM and is equivalent to DMM in HTM-16.0. For the sake of simplicity, we focus our discussion on DMM1 in this paper.

C. *Segment-wise Depth Coding (SDC)*

SDC is an alternative method of coding the residual signals in 3D-HEVC. It allows using only a CPV to represent each segment instead of quantized discrete cosine transformation (QDCT) coefficients. Generally, depth maps have noise, which makes the CPV inaccuracy to represent the current PU. Hence, an offset around original CPVs [22] are searched based on J_{vso}. After that, the rectified CPVs employ prediction coding and the delta CPVs are signaled in the bitstream. In traditional HEVC intra modes, the PU is considered only as one segment and there are two segments in DMM1.

D. *Depth Intra Mode Decision and its Complexity Analysis*

In Fig. 2, the flow chart of the default depth intra mode decision in HTM-16.0 is illustrated. The shaded blocks in Fig. 2 are the processes to be modified by our proposed algorithm to speed up HTM-16.0. The main processes of the depth intra mode decision are summarized in the following five steps:

Step 1. The rough mode decision (RMD) algorithm is employed to select several HEVC intra mode candidates (3 modes for 64×64, 32×32 and 16×16 PUs, and 8 modes for 8×8 and 4×4 PUs) [24] roughly by minimizing the low complexity RD-Cost (simplified as $LCRD_{cost}$) as

$$LCRD_{cost} = D_{VSO} + \lambda \times \mathrm{Rate}(Mode) \quad (4)$$

where the synthesis distortion D_{syn} in D_{VSO} is calculated by the VSD metric in (2). The depth distortion D_{dep} in (1) is SATD, $Rate(Mode)$ is the coding rate associated with the chosen mode, and λ is the weighting factor. Now, let us define $LCRD_{mincost}$ to be the minimum $LCRD_{cost}$ of all intra modes for each PU. And the corresponding rough mode associated with this $LCRD_{cost}$ is defined as $RM_{mincost}$. Additionally, three most probable modes (MPMs) are appended as candidates, which are predicted from the left and up neighboring PUs.

Step 2. The best-matching wedgelet partition among all the wedgelet pattern candidates is sought at the encoder by minimizing J_{vso} using the VSD-based VSO.

Step 3. A pool is constructed by the above candidates, including the rough intra modes and MPMs in Step 1 (3 to 11 candidates), and the DMM1 with the optimal wedgelet pattern in Step 2 . J_{vso} using the full complexity SVDC-based VSO with limited residual quadtree (RQT) [25] is calculated for all candidates in the pool with the traditional transform-based residual coding.

Step 4. J_{vso} using the full complexity SVDC-based VSO is calculated for all candidates in the pool again using SDC to encode the residual block. The costs from steps 3 and 4 are compared to select the final optimal intra mode and determine whether SDC or the traditional transformed-based residual coding is used.

Step 5. The full residual quadtree (RQT) is searched using the selected intra mode in step 4 to decide the optimal size of transform kernel.

Since a large amount of candidates are considered in depth intra mode decision, the depth map coding occupies about 86% of total 3D-HEVC encoding time, as illustrated in Fig. 3(a), in which all intra configuration in HTM-16.0 was used. In order to investigate the coding complexity of depth maps in more details, Fig. 3(b) illustrates the encoding time occupation for each step in depth map coding. The three most time-consuming processes are the full RD calculation of the candidates with QDCT in step 3 (29.04%), the SDC decision in step 4 (24.74%), and the optimal wedgelet pattern decision of DMM1 in step 2 (20.25%). It is noted in Fig. 3(b) that the depth intra skip mode is designed for smooth regions by pixel direct copy in both intra and inter prediction. Since it only occupies about 4.48% of the depth encoding time, this is not the major concern in this paper. Although the non-rendering VSD method is adopted in computing D_{syn} in step 2, the huge computational complexity comes from the enormous number of wedgelet pattern candidates of DMM1 as illustrated in Table I. Step 3 and 4 employs the time-consuming VSO based on SVDC for 5 to 13

TABLE I
NUMBER OF WEDGELET PATTERNS IN DMM1

PU	Full Search	Fast Algorithm in [32]
4×4	86	58
8×8	766	310
16×16	510	384
32×32	510	384

candidates, resulting in intolerable time costs. Besides, step 4 checks all the combinations of offsets for CPVs, which is another reason for high complexity. In this paper, our proposed algorithm will focus on reducing the complexities in steps 2, 3 and 4 by skipping most unnecessary candidates and providing a more simple VSO metric for DMM1 decision in step 2.

III. Related Work

The fast algorithms for depth intra mode decision can be classified into four categories: skipping DMM in step 2 for unnecessary PUs [26]-[31]; reducing the number of wedgelet patterns for DMM1 in step 2 [16]-[17], [32]-[35]; simplifying the VSO metric [19]-[20], [36]-[37] in step 3 to 5; and reducing the number of candidates and limiting the search range for SDC in step 4 [38]-[39].

The DMM skipping algorithms in [26]-[29] identify smooth regions to skip DMM. PU is considered as a smooth region when the Planar mode is selected in RMD [26]. In [27], a threshold-based DMM skipping method was further developed using the rough mode cost from RMD as the extension of [26]. The algorithm in [28] omits the DMM calculation in a smooth region when the Planar mode is one of the most probable mode. Zhang *et al*. [29] made full use of the coding information from the spatial neighboring treeblock and the co-located texture to predict the depth intra mode treeblock and early terminate the DMM mode decision process. On the other hand, the investigations in [30]-[31] were raised to skip unnecessary DMM based on simple edge regions where one of the angular modes is efficient and the redundant DMM should be avoided. In [30], an edge classification based DMM decision in Hadamard transform domain was proposed to detect the blocks with a horizontal or vertical edge. The work in [31] then proposed a simple edge detector by comparing the difference of four corner pixels with a pre-defined threshold to skip unnecessary DMM blocks. If the current PU is worth searching DMM decided by [26]-[31], all the wedgelet patterns are calculated in these algorithms. The algorithms in [16]-[17], [32]-[35] narrowed the scope of necessary wedgelet patterns that need to be searched. Merkle *et al*. [32] developed a two-steps wedgelet pattern decision algorithm, one for coarse wedgelet search in the double pixel-domain and the other for refinement. In addition, Xu *et al*. [33] paid attention to utilizing the direction mode with the minimal cost in RMD and searched in its corresponding wedgelet pattern subset. Gustavo *et al.* [34] searched the wedgelet patterns around the border samples with the largest gradient. Our prior works classify the DMM candidates into six subsets and use the variance as the feature to determine which subset should be checked [17]. In [35], a flexible block partitioning scheme was designed to combine with a constrained wedgelet pattern subset according to the partition blocks. For simplifying the VSO metric and SDC calculation, Li *et al*. [36] estimated the VSO using an adaptive model for different pixel intervals. Byung *et al*. [37] proposed an area-based scheme, which only requires co-located texture information for VSO calculation. A fast SDC decision was suggested based on the mode information of non-SDC [38]. Lee *et al*. [39] limited the search range of an offset for CPVs in the SDC decision process.

In addition to these four types of fast depth intra mode decision, Mora *et al.* [40] exploited texture-depth redundancies and developed an inter-component coding tool, in which the depth quadtree is limited to the coded texture quadtree. In [41], a RD cost-based fast algorithm was designed to skip DMM calculation and SDC testing for DMM candidates. Based on statistical analysis of intra mode, Zhang *et al.* [42] jointly reduced the number of the conventional intra mode candidates and simplified DMM decision. Furthermore, recent fast algorithms [43] were also proposed to reduce the complexity of texture coding in 3D-HEVC.

Meanwhile, the methods in [19]-[20], [26], [32], [38]-[40] have been adopted by HTM-16.0 [22]. However, the complexity requirement of depth intra mode decision is still huge, and there is plenty of room for improvement. It is noted that the quadtree limitation of [40] is switched off for intra slices in HTM-16.0 since it damages the synthesized view quality significantly and causes decoder decoupling. Interested readers may refer to references [44]-[45]

IV. Proposed Algorithm of Fast Depth Intra Mode Decision

Compared with previous research works, our contributions are as follows: We propose (i) a very low-complexity VSO metric for wedgelet pattern decision in DMM1 in which the time consuming J_{vso} is entirely replaced by calculating the variances of two segments for each candidate pattern, and (ii) a probability-based early depth intra mode decision (PBED) scheme to skip the unnecessary conventional intra mode and DMM1 by selecting the most probable intra mode candidates based on the low-complexity RD-Cost in RMD. More importantly, the new low-complexity VSO metric for DMM1 decision can work well with the proposed PBED to speed up depth intra mode decision further. It can also be used with other existing fast algorithms.

A. New VSO metric of DMM1 decision

1) Statistical properties of optimal wedgelet pattern

Obviously, DMM1 is a mean method to describe the PU, in which each segment can be represented by one constant pixel value (CPV) as mentioned in Section II. There are two situations that DMM1 is beneficial to depth map coding. First, when an irregular sharp edge exists in a certain CU, the conventional intra mode with only one direction cannot provide a good prediction for a sharp edge. As a result, the coding artifacts may appear around the sharp edge or this CU may be partitioned into four sub-CUs for finding more exact description of the sharp edge, which increases the bit cost for partition information. Therefore, in this situation, DMM1 is superior to the conventional intra modes since it can efficiently represent the irregular sharp edge by one of the wedgelet patterns. Second, depth maps, typically, have noise especially in sequences generated by depth estimation. Here, we consider the mode decision as the pixels classification. For these noisy regions, the 33 angular intra modes in Fig. 1(a) cannot achieve a decent prediction for taking all pixels into account. Therefore,

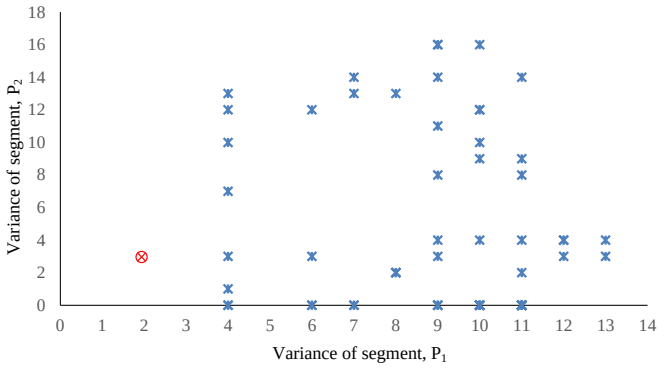

Fig. 4. Example of variance distribution for two segments in DMM1 for a given 4×4 PU.

TABLE II
NUMBER OF OPERATIONS FOR TESTING ONE WEDGELET PATTERN CANDIDATE USING DIFFERENT VSO METRIC.

Operation		+ or−	× or ÷	<or>	| • |
VSO	VSD	$5N^2$	$5N^2$	N^2	$3N^2$
	SSE	N^2	N^2	-	-
	Total	$6N^2$	$6N^2$	N^2	$3N^2$
SEDV		$3N^2$	N^2	-	-

the mean methods, including Planar, DC or DMM1, can give smaller distortion for PUs. However, the planar mode is for PUs with gradually changing pixel values and the DC mode is for smooth PUs in which all pixels around one CPV. On the other hand, when the polluted PUs have two CPVs and can be broadly considered as piece-constant PU, DMM1 makes an excellent complement to describe these PUs. For these two situations, the optimal wedgelet pattern in DMM1 also tends to delimit the similar pixels into the same segment. Consequently, it can be assumed that the pixel variances of two segments in the optimal wedgelet pattern are smallest among all the other patterns. The example in Fig. 4 could be used to demonstrate this assumption. The x-axis and y-axis denote the variance values of two segments, P_1 and P_2, respectively. Each point stands for a wedgelet pattern candidate, the one denoted by red ⊗ is the optimal wedgelet pattern. It can be seen that the best wedeglet pattern is nearest to (0,0) among all candidates. This can be used to find the final wedgelet pattern, which inspires us to develop a new VSO metric for DMM1 decision instead of the VSD-based VSO calculation using (1) and (2). From Fig. 1(b), a straight line L_{SE} separates the block into two segments P_1 and P_2. In our algorithm, the variances of pixels in P_1 and P_2 are utilized to measure the similarity of pixels within the segments, and let us denotes as

$$Var_{P1} = \sum_{i \in P1} (f_i - CPV_{P1})^2 \tag{5}$$

and

$$Var_{P2} = \sum_{i \in P2} (f_i - CPV_{P2})^2 \tag{6}$$

where f_i is the pixel value within the segment. CPV_{P1} and CPV_{P2} are the constant pixel values to describe the two segments, which are also the mean values of all pixels in P_1 and P_2, respectively. To find the wedgelet pattern that has the smallest Var_{P1} and Var_{P2} simultaneously, we employ the

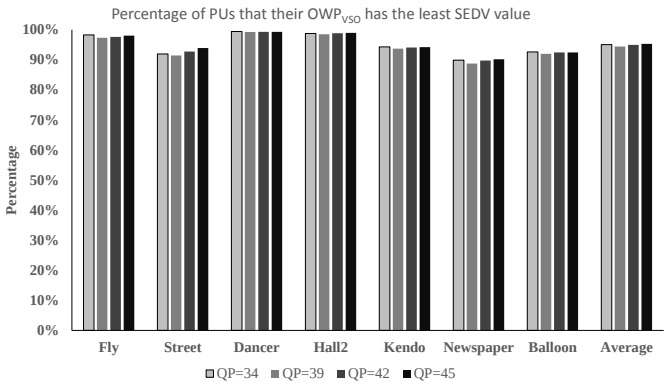

Fig. 5. Percentage of PUs that have the least SEDV value in OWP_{VSO}.

Algorithm 1: SEDV-based VSO for DMM1 decision

Input: an N×N PU, $SEDV_{best}$ = Maximum
for each wedgelet pattern WP_i **do**
Calculate the CPV_1 and CPV_2 for segments P_1 and P_2;
Calculate the SEDV for WP_i by (7);
if ($SEDV(WP_i) < SEDV_{best}$) **then**
$SEDV_{best} \leftarrow SEDV(WP_i)$;
$WP_{best} \leftarrow WP_i$;
end if
end for
Output: Best wedgelet pattern WP_{best}

Algorithm 2: VSD-based VSO for DMM1 decision

Input: an N×N PU, J_{Best} = Maximum
for each wedgelet pattern WP_i **do**
Calculate CPV_1 and CPV_2 for segment P_1 and P_2;
Get the reconstructed depth using CPV_1 and CPV_2;
Calculate J_{vso} for WP_i ($J_{VSO}(WP_i)$) using VSD- based VSO by (1) and (2);
if ($J_{vso}(WP_i) < J_{Best}$) **then**
$J_{Best} \leftarrow J_{vso}(WP_i)$;
$WP_{best} \leftarrow WP_i$;
end if
end for
Output: Best wedgelet pattern WP_{best}

squared Euclidean distance of two variances, SEDV, for segments in DMM1 as

$$SEDV = Var_{P1}^{\ 2} + Var_{P2}^{\ 2} \tag{7}$$

In order to investigate the relationship between the VSD-based VSO and SEDV, the optimal wedgelet pattern determined by the VSD-based VSO in 3D-HEVC is defined as OWP_{VSO} for the sake of convenience, and the SEDV of all wedgelet patterns for different sequences with four QPs are examined carefully. It is found that about 90%-99% of PUs has the least SEDV value in OWP_{VSO} as shown in Fig. 5. It verifies our assumption that the optimal wedeglet pattern groups the similar pixels together. Therefore, the simple SEDV metric can entirely replace the time-consuming VSD-based VSO safely in DMM1 decision of Step 2 in Section II-D.

2) Adoption of SEDV metric into DMM1 decision

According to the above analysis of SEDV, the detailed

implementation of the proposed wedgelet pattern decision algorithm is explained by the pseudo-code **Algorithm 1**, while the pseudo-code **Algorithm 2** is the original VSD-based VSO. Given an $N \times N$ PU, Var_{P1} and Var_{P2} in (5) and (6) are calculated for all wedgelet pattern candidates. Then, all SEDV values are computed based on (7). The wedgelet pattern with minimal value of SEDV is selected as the final optimal one. It is noted that the SSE calculation for D_{dep} in (1) can also be skipped when the SEDV-based VSO is adopted. In the calculation of SEDV in (7), one multiplication and three addition/subtraction operations for each pixel are required. Therefore, for an $N \times N$ PU, the computation complexity of SEDV is N^2 multiplication and $3N^2$ addition/subtraction operations for testing one wedgelet pattern. On the other hand, the original VSD-based VSO gets the reconstructed depth block Rec_D using CPV_{P1} and CPV_{P2}. Then the calculations of VSD and SSE for D_{syn} and D_{dep}, respectively, require five and one multiplication operations for each pixel. Besides, there are additional five and one addition/subtraction operation to compute VSD and SSE for each pixel. Altogether the VSD-based VSO needs $6N^2$ multiplication operations and $6N^2$ addition operations for an $N \times N$ PU. In (2), it can be found that there are three absolute operations for computing the VSD metric and one relational operation for W_d per sample. Table II illustrates the total operations required in the proposed and original algorithms for one wedgelet pattern candidate. By considering the number of wedgelet pattern candidates in Table I, the VSO calculation needs to be computed a huge number of times for a given PU. Obviously, the required multiplication and addition/subtraction operations of the proposed metric are 6 times and 2 times, respectively, lower than those of the VSD metric. In addition, the proposed SEDV metric need not involve any absolute and relational operations. By taking this into account, the computational requirement of the proposed SEDV-based VSO is much lower than that of the VSD-based VSO for wedgelet pattern decision. It is interesting to note that the complexity reduction is independent of the number of wedgelet patterns, the proposed low-complexity SEDV metric can then be integrated into the other algorithms which can reduce the number of wedgelet pattern candidates [26].

B. Probability-based early depth intra mode decision

The proposed SEDV-based VSO algorithm can reduce the complexity of selecting the best-matching wedgelet partition in DMM1. From Fig. 3(b), it can be observed that steps 3 and 4 in depth intra mode decision also takes up most resources, and should be noteworthy. Skipping the complexity of these steps for depth intra coding is more effective and strongly desirable. Therefore, in this subsection, a probability-based early depth intra mode decision (PBED) is proposed to select the most probable intra mode candidates based on the low complexity RD-Cost in RMD from step 1.

1) Correlation between $LCRD_{mincost}$ and final intra mode

Depth maps always consist of mostly smooth regions and have a strong direction at edges. Due to these two characteristics, the intra prediction of depth maps could be very accurate, which leads to a zero-biased distribution of RD-Cost

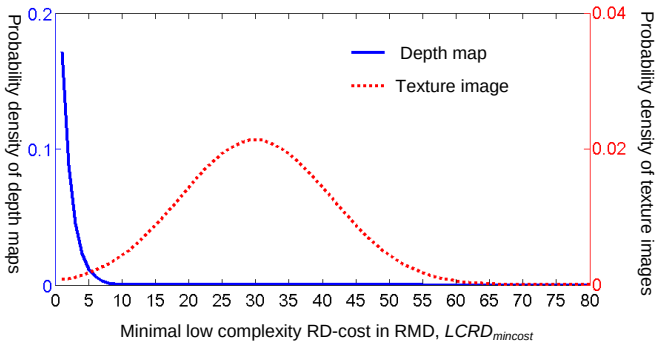

Fig. 6. Probability density functions of $LCRD_{mincost}$ for depth maps and texture images.

in depth maps. Similarly, it is observed that $LCRD_{mincost}$ calculated in RMD is also zero-biased. On the contrary, $LCRD_{mincost}$ of coding texture images follows a Gaussian distribution as described in [46]. Fig. 6 shows the probability density functions of $LCRD_{mincost}$ for depth maps and texture images. The solid curve denotes the probability density function of depth maps aligned with the principal y-axis, and the dotted curve represents that of texture images aligned with the secondary y-axis. From these results, we can confirm that $LCRD_{mincost}$ of depth maps has a zero-biased distribution. If $RM_{mincost}$ (the best rough mode associated with $LCRD_{mincost}$, as defined in Section II-D) can predict the PU well, the other candidates can be skipped after the RMD process. Hence, we construct a classifier using $LCRD_{mincost}$ by RMD. Inspired by this, we investigate the rough modes by RMD and their low-complexity costs statistically. The relationships between $RM_{mincost}$ and the final optimal intra mode of the *Balloons* sequence with different quantization parameters (QPs) are plotted in Fig. 7. In Fig. 7, the symbol $P_{rm}(F/x= X_0)$ denotes the conditional probability of $RM_{mincost}$ to be the final optimal intra prediction mode given that $LCRD_{mincost}$ equals to X_0. The PUs could be classified by the corresponding $LCRD_{mincost}$ in terms of mode selection. When proper threshold $TH_{mincost}$ is selected as specified by the red dot line in Fig. 7, $P_{rm}(F/x=X_0)$ can reach more than 98%, given the $LCRD_{mincost}$ is smaller than $TH_{mincost}$. From Fig. 7, it can be seen that $TH_{mincost}$ should be made adaptive to QP, and will be discussed later. The statistics in Fig. 7 convincingly verifies that the final optimal intra mode is strongly correlated with the value of $LCRD_{mincost}$.

2) Correlation between $LCRD_{mincost}$ and SDC

After constructing the classifier using $LCRD_{mincost}$, most of intra mode candidates should be skipped. However, the selected candidate is still encoded twice with non-SDC in step 3 and SDC in step 4 using the SVDC-based VSO. In order to reduce the complexity introduced by SDC, we further investigate the relationship between $LCRD_{mincost}$ and SDC as depicted in Fig. 8. The symbol $P_{sdc}(F/x=X_0)$ in Fig. 8 denotes the conditional probability of $RM_{mincost}$ adopting SDC to encode the residual block. With the same threshold in Fig. 7, about 95% percentage of PUs also use SDC when their $LCRD_{mincost}$ are smaller than $TH_{mincost}$. It is due to the reason that the selected mode can predict well for most pixels in the current PU and the prediction for a residual signal can provide the good synthesized view quality by a consistent difference of disparities. Therefore,

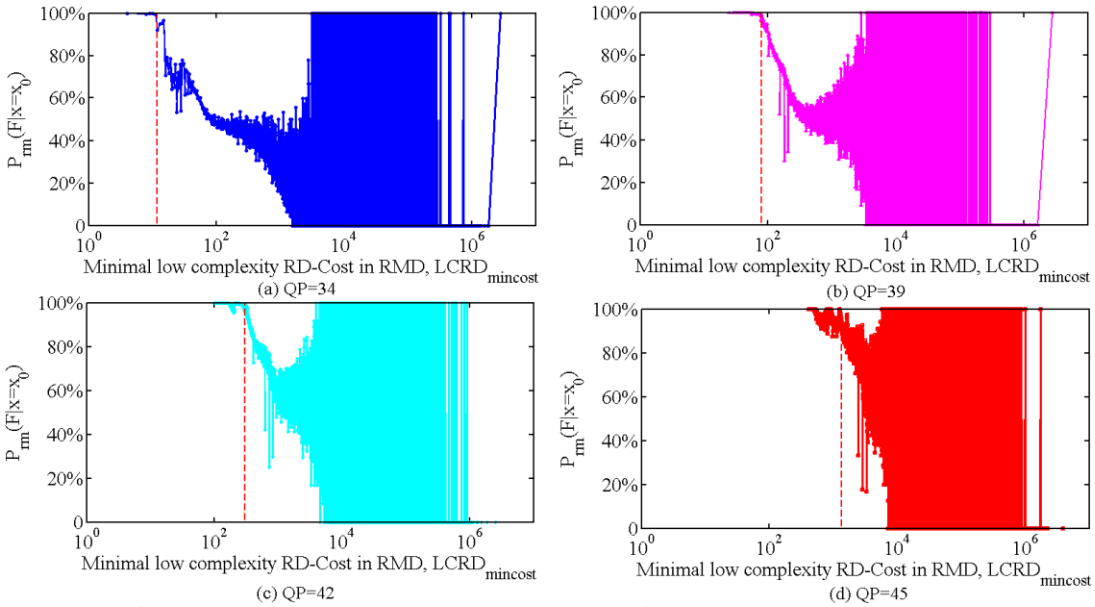

Fig. 7. Conditional probability of $RM_{mincost}$ in *Balloons* as the optimal intra prediction mode for the given $LCRD_{mincost}$ in RMD: (a) QP=34, (b) QP=39, (c) QP=42, and (d) QP=45.

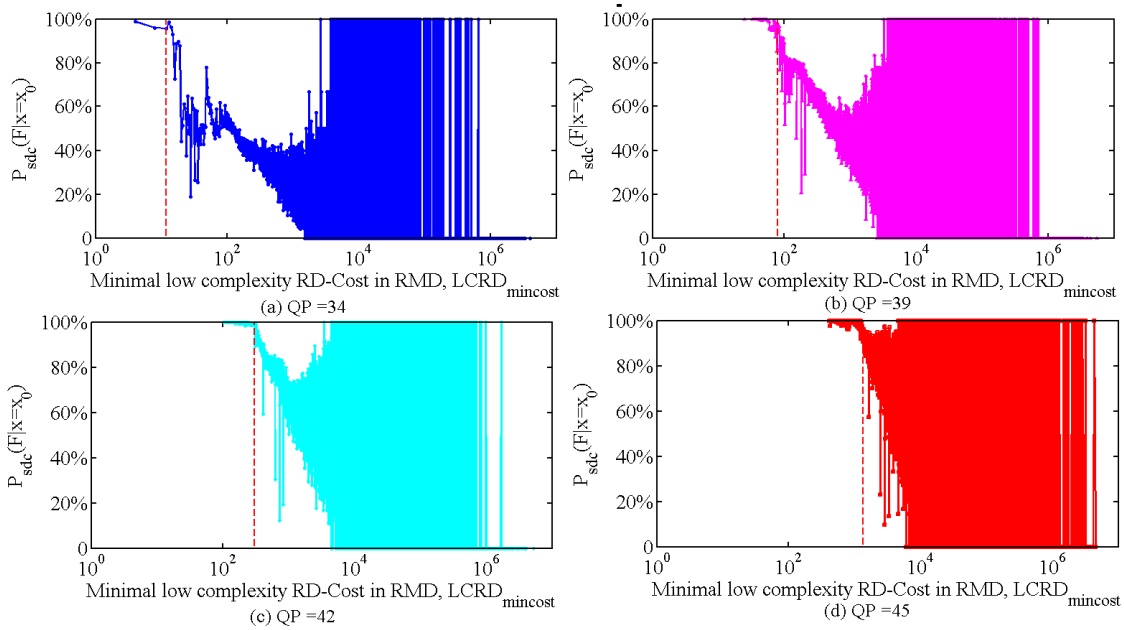

Fig. 8. Conditional probability of $RM_{mincost}$ in *Balloons* using SDC to encode the residual for the given $LCRD_{mincost}$ in RMD: (a) QP=34, (b) QP=39, (c) QP=42, and (d) QP=45.

$LCRD_{mincost}$ also has high correlation with SDC. In the PUs with small $LCRD_{mincost}$, the checking of non-SDC can be skipped. It means that the high complexity SVDC-based VSO in step 3 for transform-based residual coding can be saved, resulting in further reducing the complexity of depth intra coding. Extensive simulations show that other sequences provide similar distributions of $P_{rm}(F/x=X_0)$ and $P_{sdc}(F/x=X_0)$ in Fig. 7 and Fig. 8. In Fig. 9, the probability distribution of PUs with different $LCRD_{mincost}$ is shown. It can be seen that huge amount of PUs have smaller $LCRD_{mincost}$ and are likely to be well predicted by $RM_{mincost}$. As a result, a substantial reduction in complexity could be expected if $LCRD_{mincost}$ in RMD is well exploited. The same thresholds as in Fig. 7 and Fig. 8 show that large percentage of PUs belong to low-cost cases, where substantial reduction could be achieved. In fact, when the well-constructed depth maps of the sequences such as *GT_Fly* and *Ponan_Hall2* are intra coded, the percentage of accurate prediction is even higher. Consequently, $LCRD_{mincost}$ of PUs is found to be highly correlated with the final optimal intra modes as well as SDC and can be used to early terminate the process of depth intra mode decision.

3) Determination of threshold for PBED

Our proposed PBED algorithm determines the most probable intra mode candidate by exploiting the relation between $LCRD_{mincost}$ and the final optimal intra mode before calculating J_{vso}. It also makes an early decision that whether SDC is directly used instead of transform-based residual coding by exploiting the relation between $LCRD_{mincost}$ and SDC usage among all PUs. As a result, the time consuming of both the regular intra modes, DMM1 as well as SDC decision are

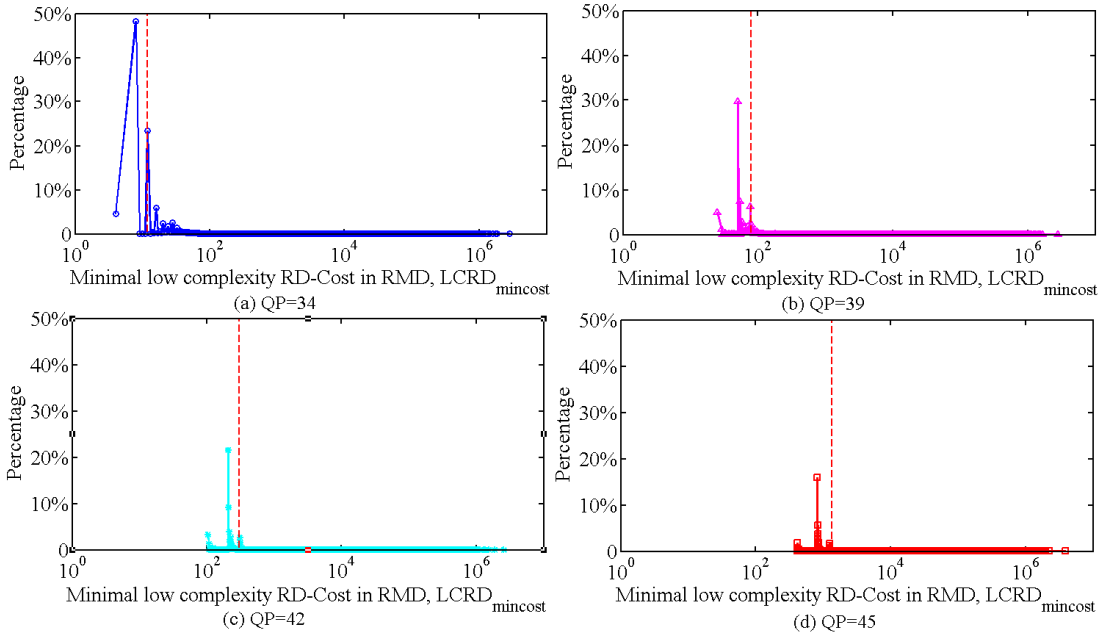

Fig. 9. Probability distributions of PUs with different $LCRD_{mincost}$: (a) QP=34, (b) QP=39, (c) QP=42, and (d) QP=45.

reduced significantly. In order to better trade-off between the time reduction and coding performance, the threshold $TH_{mincost}$ in the proposed PBED algorithm is determined carefully. From Fig. 7 and Fig. 8, it can be observed that $TH_{mincost}$ depends on QP. By considering (4), $LCRD_{cost}$ is related to the depth map distortion, the sum of gradients in texture, the bit cost for the chosen mode and the Langrage Multiplier λ. To enable VSO, a scaled λ technique is required to adjust λ by a factor $F(QP)$ depending on QP [22]. The scaled Lagrange Multiplier λ_s is then equal to $\lambda \times F(QP)$, where $F(QP)$ is from 0.0313 to 0.8 indexed by QP. This Lagrange Multiplier scaling technique is also applied into (4) to calculate $LCRD_{cost}$. Hence, the value of the final $LCRD_{mincost}$ should also be related to λ_s, the distortion and bit cost. Besides, the original λ is indexed by QP as $0.57 \times 2^{(QP-12)/3}$. Fig. 10 shows the original and scaled Lagrange Multiplier for QP from 0 to 51. We thus consider $TH_{mincost}$ as a linear equation $D+\lambda_s \times B$, where D is the distortion, and B is the bit cost. Hence, the linear equation should be adaptively determined by these two parts for different bitrate scenarios. It is noted that the use of a linear equation to determine the threshold is well established in intra mode decision for texture coding [47]-[48]. Interested readers are encouraged to read [47]-[48]. In this paper, we further extend this concept to derive the threshold value of our proposed PBED in depth map coding. From Fig. 10, we can see that a small value of QP corresponds to a small λ_s. In this high bitrate scenario, B has nearly no effects on the value of $LCRD_{mincost}$. A constant $TH_{mincost}$ that solely depends on D can then be adopted in our proposed algorithm. λ_s increases with QP and is equal to 1 at QP=30, the constant $TH_{mincost}$ is applied to the case that QP is smaller than or equal to 30. Based on the results of extensive simulations, D is set to 30 empirically, which can obtain a better tradeoff between the computational complexity and coding performance. On the other hand, in low bitrate scenario, λ_s has a larger value, it indicates that B plays a critical role in the calculation of $LCRD_{mincost}$. Hence, the determination of $TH_{mincost}$ takes both of D and B into consideration, which becomes $D+\lambda_s \times B$. It is noted that the signaling of the intra mode adopts the MPM strategy. If the selected mode is MPM, only 2-bit or 3-bit index is transmitted, otherwise, 6 fixed bits are required for the remaining intra modes. In this paper, B is therefore set to 6 for $TH_{mincost}$ in this case. It implies that the proposed algorithm

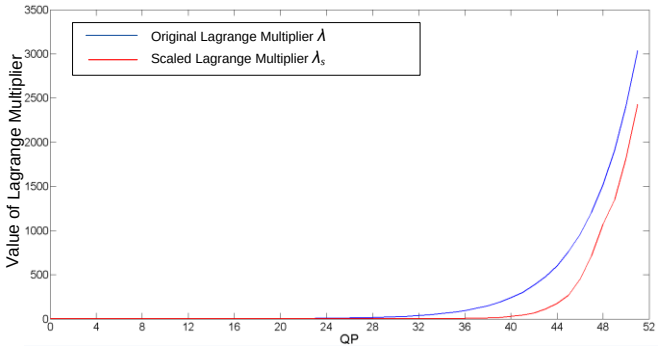

Fig. 10. Values of λ and λ_s for different QP.

Algorithm 3 Proposed overall (SEDV+PBED) algorithm

Input: an N×N PU
Employ the rough mode decision process;
Obtain $LCRD_{mincost}$ and $RM_{mincost}$;
Calculate the threshold $TH_{mincost}$ by (8) ;
if ($LCRD_{mincost} < TH_{mincost}$) **then**
  SDC decision for $RM_{mincost}$
else
  Employ the SEDV-based VSO for DMM1 decision
  Candidate pool construction: 3 to 11 RMs and DMM1
  for each mode in candidate pool **do**
    Calculate J_{vso} using SVDC-based VSO without SDC
    Calculate J_{vso} using SVDC-based VSO with SDC
  end for
end if
Calculate the full RQT for the best intra mode
Output: Best intra mode and SDC flag

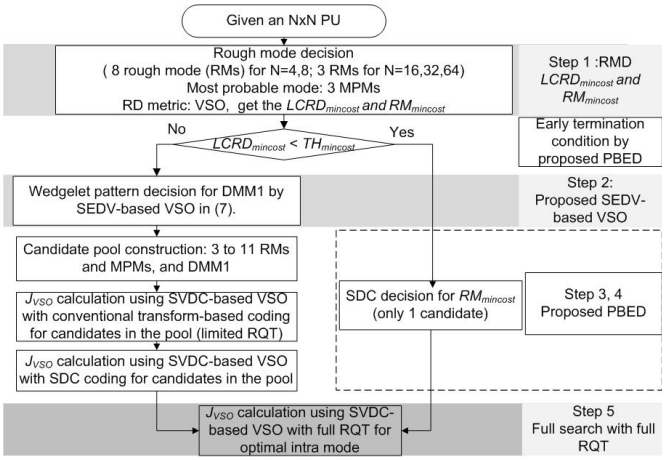

Fig. 11. Flow chart of integration of SEDV metric into PBED.

tolerates more distortion (about $3\lambda_s$ or $4\lambda_s$) for MPMs and is more inclined to select them to be the optimal intra mode. In conclusion, the piecewise threshold strategy is defined according to QP index as

$$TH_{mincost} = \begin{cases} D & , \ QP \le 30 \\ D + 6 \times \lambda_s, & QP > 30 \end{cases} \tag{8}$$

C. Integration of SEDV metric into PBED

In this subsection, the simple SEDV-based VSO scheme for fast DMM1 decision, and the probability-based early depth intra mode decision (PBED) scheme for skipping unnecessary candidates and SDC, are integrated together to achieve low complexity depth intra mode decision in 3D-HEVC. The flow chart of the proposed integration is shown in Fig. 11 and the detailed implementation of the proposed integration is explained by the pseudo-code **Algorithm 3**. Given a PU with the size of N×N, some rough modes and their $LCRD_{cost}$ are obtained after rough mode decision. The minimal $LCRD_{cost}$ is used to classify the PUs into two categories. If the PUs are satisfied with the proposed early termination condition ($LCRD_{mincost} < TH_{mincost}$), only the $RM_{mincost}$ (1 candidate) is selected as the final optimal intra mode and all the other candidates are skipped. After obtaining the intra mode, the residual is directly employed SDC coding without non-SDC checking for the selected candidate. In other words, there is no need to employ the process of depth intra mode decision for SVDC-based VSO with the conventional transform-based residual coding (step 3 in Section II-D). All the other candidates in the pool including the conventional intra modes and DMM1 are skipped (step 4 in Section II-D) for complexity saving. Notice that the process of searching the optimal wedgelet pattern for DMM1 (step 2 in Section II-D) is also skipped entirely since no DMMs are required in this case. Only the optimal SDC offset of CPVs is searched for only one candidate. If the early termination condition does not meet, the proposed SEDV-based VSO is employed to find the optimal wedgelet pattern. The intra mode candidates, including 3 to 11 rough modes and DMM1 are performed by calculating J_{VSO} for SDC and non-SDC decision.

TABLE III
IMPORTANT PARAMETERS FOR DEPTH CODING

DMM	Enabled	Fast SDC decision [38]	Enabled
SDC	Enabled	Fast DMM decision [26]	Enabled
DLT	Enabled	Fast DMM1 [32]	Enabled
VSO	Enabled	Entropy coding	CABAC
VSD	Enabled	RMD [24]	Enabled
RQT	Enabled	Fast SDC decision [39]	Enabled

V. SIMULATION RESULTS

To evaluate the performances of the proposed SEDV-based VSO and PBED, they have been implemented in the reference software HTM-16.0 of the 3D-HEVC standard [49]. Several sequences with two resolutions of 1920×1088 and 1024×768 recommended by the JCT-3V group were encoded. They include *Poznan_Hall2*, *Poznan_Street*, *Undo_Dancer*, *GT_Fly* and *Shark* (1920×1088) as well as *Kendo*, *Balloons* and *Newspaper1* (1024×768). The quantization parameters were set to {(25, 34), (30, 39), (35, 42) and (40, 45)} for coding texture videos and depth maps, respectively. About 200 to 300 frames were tested for each sequence under the common test conditions (CTC) specified in [50]. Some important encoding parameters in this document are tabulated in Table III. It is noted that the view synthesis optimization (VSO) and the model-based synthesized view distortion estimation (VSD) were enabled. In the following simulations, all the fast algorithms listed in Table III are activated. Since the proposed techniques focus on depth intra coding, all test sequences were encoded using the intra-only structure. Three views, V_0, V_1 and V_2, for each sequence were encoded and six synthesis intermediate views, from $V_{0.25}$ to $V_{1.75}$, were rendered at decoder side. For PBED, *D* was set to 30 for all sequences. The objective evaluation of video quality is calculated by the average difference of bitrate (ΔBDBR), which comes from Bjontegaard metrics [51] presenting the rate distortion performance of the synthesis view quality and the total bitrate including texture and depth videos. ΔT (%) represents depth coding time change in percentage as compared with the benchmarking algorithms, which is defined as

$$\Delta T = \frac{DT_{Reference} - DT_{HTM-16.0}}{DT_{HTM-16.0}} \times 100\% \tag{9}$$

where $DT_{HTM\text{-}16.0}$ is the depth encoding time in HTM-16.0 software, and $DT_{Reference}$ denotes the depth encoding time of

TABLE IV
BD PERFORMANCE AND TIME SAVING OF HTM-16.0 WITHOUT DMM1 COMPARED WITH THE CASE WITH DMM1.

Test seq.	ΔBDBR (%)						ΔT(%)
	$V_{0.25}$	$V_{0.5}$	$V_{0.75}$	$V_{1.25}$	$V_{1.5}$	$V_{1.75}$	
Kendo	2.78	3.18	1.88	1.99	3.86	3.81	-27.18
Balloons	7.43	9.09	8.78	6.83	7.98	7.52	-28.18
Newspaper1	10.92	10.55	7.95	4.98	7.40	5.18	-29.38
1024×768	**7.04**	**7.61**	**6.20**	**4.60**	**6.42**	**5.50**	**-28.25**
Undo_Dancer	7.39	9.29	7.42	7.66	9.20	6.57	-26.01
GT_Fly	1.78	2.36	1.91	1.91	2.49	1.85	-25.86
Poznan_Hall2	5.54	8.02	4.56	7.74	5.93	3.68	-20.45
Poznan_Street	1.95	2.92	2.07	2.30	3.69	2.28	-26.09
Shark	5.01	6.70	5.58	5.33	6.44	4.74	-27.10
1920×1088	**4.16**	**5.65**	**3.99**	**4.90**	**5.33**	**3.59**	**-24.60**
Avg.	**5.40**	**6.49**	**4.94**	**4.77**	**5.79**	**4.41**	**-26.17**

TABLE V
BD PERFORMANCE AND TIME SAVING OF THE PROPOSED SEDV-BASED VSO COMPARED WITH HTM-16.0

Test sequence	ΔBDBR (%)						Time change of wedgelet pattern decision (%)				ΔT (%)			
	$V_{0.25}$	$V_{0.5}$	$V_{0.75}$	$V_{1.25}$	$V_{1.5}$	$V_{1.75}$	34	39	42	45	34	39	42	45
Kendo	0.21	0.35	0.26	0.18	0.25	0.21	-68.51	-68.70	-68.73	-68.46	-13.84	-13.41	-11.52	-9.15
Balloons	0.16	0.29	0.15	0.15	0.21	0.13	-68.23	-68.61	-68.40	-68.44	-13.37	-12.79	-10.47	-9.33
Newspaper	0.39	0.55	0.42	0.39	0.46	0.30	-70.69	-70.42	-70.03	-69.83	-14.80	-13.37	-10.71	-9.79
1024×768	**0.25**	**0.39**	**0.28**	**0.24**	**0.31**	**0.21**	**-69.14**	**-69.24**	**-69.05**	**-68.91**	**-14.00**	**-13.19**	**-10.90**	**-9.42**
Undo_Dancer	0.08	0.07	0.10	0.10	0.10	0.07	-70.10	-70.26	-70.34	-70.01	-15.27	-12.12	-8.77	-6.53
GT_Fly	0.15	0.16	0.13	0.14	0.16	0.12	-69.39	-69.74	-68.67	-70.45	-16.95	-14.29	-7.92	-5.17
Poznan_Hall2	0.28	0.37	0.30	0.22	0.41	0.22	-71.03	-71.99	-71.69	-71.44	-12.98	-11.34	-6.72	-6.29
Poznan_Street	0.10	0.18	0.11	0.15	0.19	0.14	-70.30	-69.77	-70.23	-69.69	-14.46	-13.51	-8.33	-6.86
Shark	0.09	0.12	0.11	0.08	0.09	0.04	-69.50	-69.38	-69.40	-69.40	-15.74	-14.21	-10.10	-9.58
1920×1088	**0.14**	**0.18**	**0.15**	**0.14**	**0.19**	**0.12**	**-70.06**	**-70.23**	**-70.06**	**-70.20**	**-15.08**	**-12.06**	**-9.40**	**-6.88**
Avg.	**0.18**	**0.26**	**0.20**	**0.18**	**0.23**	**0.15**	**-69.75**	**-69.93**	**-69.73**	**-69.76**	**-14.53**	**-12.24**	**-9.94**	**-7.59**

reference algorithms. Positive and negative values denote increments and decrements, respectively. The simulations were conducted on a 64-bit MS Windows 7 OS running on an Intel Xeon(R) E3-1230 CPU of 3.3 GHz and 16.0GB RAM

A. Performance of DMM1

Since the new DMM or DMM1 tool has been changed significantly through the standardization process, we first evaluate the performance of DMM1 in the current HTM-16.0 as compared to the case without DMM1. Table IV shows that the use of DMM1 can achieve about 5% BDBR saving. This results show that DMM1 is an inevitable technique to provide a high compression rate for depth intra coding. At the same time, about 26% complexity is brought by DMM1, which is dramatically reduced compared with that in the previous versions of HTM, e.g. 78% in HTM-3.0 [33] and 40% in HTM-8.1 [17]. Despite this great reduction in complexity, the coding burden introduced by DMM1 for depth intra coding is still large in the current test model. On the other hand, the endeavor to simplification of DMM1 has being achieved throughout the 3D-HEVC standardization by reducing DMM1 candidates and adopting some fast methods in [26], [32] and [38]. That is why some previous approaches based on the old versions of HTM have no remarkable effect on the current test model.

B. Performance of proposed SEDV-based VSO

Table V shows the coding performance of the proposed simple SEDV-based VSO in DMM1 decision. From this table, the proposed SEDV-based VSO can provide about 70% time reduction of wedgelet pattern decision. The time savings are very similar for four different QPs. The reason is that the calculation of SEDV in our method can save 83% multiplications as compared with the VSD-based VSO metric. Therefore, time change of wedgelet pattern decision in Table V approaches the theoretical value. Meanwhile, the proposed algorithm can save 7%-14% of the depth coding time as illustrated in Table V for different QPs. Since the method [26] in HTM-16.0 skips the DMM1 using a threshold depending on QP, the percentage of PUs for skipped DMM1 becomes higher at larger QP as shown in Table VI. Therefore, the total time savings achieved by SEDV-based VSO is decreased when the QP is larger as shown in Table V. From Table V, the proposed algorithm only sacrifices 0.2% BDBR of synthesized views on average, which are neglected. Since the state-of-the-art methods in [26] and [32] have been adopted by HTM-16.0, the simulation results in Table V can also certify that the proposed SEDV-based VSO scheme can be integrated into algorithms that skip DMM1 or reduce the number of wedgelet patterns, such as [26], [32] and our proposed PBED.

TABLE VI
PERCENTAGE OF PUS FOR SKIPPED DMM1 IN HTM-16.0 AND PROPOSED PBED

Test Sequence	Method in [26]+[32] (%) (HTM-16.0)				Proposed PBED (%)			
QP	34	39	42	45	34	39	42	45
Kendo	44.0	44.7	54.5	60.0	68.0	68.7	76.4	82.9
Balloons	38.9	41.0	51.7	56.5	62.4	63.5	72.0	77.8
Newspaper1	23.1	26.7	45.0	51.3	46.5	50.2	64.9	73.7
1024×768	**35.3**	**37.4**	**50.4**	**55.9**	**59.0**	**60.8**	**71.1**	**78.1**
Undo_Dancer	37.5	52.2	66.1	73.1	67.0	74.0	84.6	89.1
GT_Fly	21.3	33.6	66.1	78.4	51.9	60.0	80.5	93.8
Poznan_Hall2	55.5	57.9	72.1	77.3	82.0	84.4	92.5	95.8
Poznan_Street	19.6	28.1	61.4	68.3	44.7	55.5	77.8	88.1
Shark	34.9	40.4	56.9	59.4	53.4	55.0	70.6	76.9
1920×1088	**33.8**	**42.4**	**64.5**	**71.3**	**59.8**	**65.8**	**81.2**	**88.7**
Avg.	**34.5**	**39.9**	**57.5**	**63.6**	**59.4**	**63.3**	**76.2**	**83.4**

C. Performance of PBED

Table VII then tabulates ΔBDBR and ΔT of the proposed PBED algorithm as compared with HTM-16.0. For PBED, *D* was set to 30 for all sequences. It can be found that PBED can achieve about 33% complexity reduction, which can be benefited from two contributions, including skipping DMM1 and the conventional intra mode, and testing SDC only. Table VI shows the comparison of the percentage of PUs for skipped DMM1 between HTM-16.0 and PBED. Our proposed PBED

TABLE VII
SIMULATION RESULTS OF PROPOSED PBED COMPARED WITH HTM-16.0

Test sequence	ΔBDBR (%)						ΔT(%)
	$V_{0.25}$	$V_{0.5}$	$V_{0.75}$	$V_{1.25}$	$V_{1.5}$	$V_{1.75}$	
Kendo	0.10	0.16	0.13	0.18	0.28	0.31	-32.00
Balloons	0.67	0.74	0.49	0.39	0.53	0.42	-28.39
Newspaper	0.76	0.85	0.83	0.44	0.54	0.29	-26.45
1024×768	**0.51**	**0.58**	**0.48**	**0.34**	**0.45**	**0.34**	**-28.94**
Undo_Dancer	0.47	0.70	0.55	0.34	0.61	0.37	-36.01
GT_Fly	0.05	0.17	0.07	0.09	0.19	0.09	-36.63
Poznan_Hall2	0.26	0.67	0.28	0.43	0.45	0.11	-44.84
Poznan_Street	0.16	0.14	0.09	0.10	0.19	0.06	-33.35
Shark	0.23	0.37	0.24	0.27	0.34	0.23	-24.99
1920×1088	**0.23**	**0.42**	**0.25**	**0.24**	**0.36**	**0.16**	**-35.16**
Avg.	**0.35**	**0.49**	**0.35**	**0.28**	**0.40**	**0.23**	**-33.95**

TABLE VIII
INFLUENCE OF D IN PBED

D	ΔBDBR (%)	ΔT(%)
0	0.24	-29.05
10	0.29	-31.18
30	**0.34**	**-33.95**
50	0.40	-34.39
70	0.44	-35.42
90	0.49	-36.24

selects a steady feature, LCRD, which can skip DMM1 calculation for about 60%-83% PUs. Compared with HTM-16.0, more than about 20% PUs can be benefited from PBED without DMM1 calculations. Besides, PBED only selects one candidate for SDC calculation.

In the following, we discuss the influence of *D* on the performance of the proposed PBED algorithm. As mentioned in Section IV-B-3, *D* is always a tradeoff between the computational complexity and coding performance. The evidence can be seen in Table VIII where the average performances of all the sequences recommended by CTC in terms of ΔT and ΔBDBR for various *D* are shown. As expected, the complexity reduction increases and the coding performance deceases as *D* increases. Besides, Fig. 12(a) and (b) depicts the detailed simulation results on ΔBDBR and ΔT for various videos at QP=34, respectively. In Fig.12 (a), it can be observed that different sequences with diverse content have different slopes. In particular, the slopes of ΔBDBR in *Newspaper* and *Balloons* are steep since the depth and texture content are more complicated. As a result, the depth distortion may degrade the synthesized view quality significantly [20]. Meanwhile, the mode decision of the complicated PUs usually are difficult to be predicted and their $LCRD_{mincost}$ always has a large value such that an increase in *D* will affect ΔBDBR significantly. On the contrary, the slopes of ΔBDBR in *Kendo* and *GT_Fly* are less steep. It is due to the fact that more PUs has a small value of $LCRD_{mincost}$. In this case, ΔBDBR is less sensitive to *D* and $LCRD_{mincost}$ becomes a stable feature for depth intra mode decision. With respect to ΔT in Fig. 12(b), it is found that there is considerable discrepancy of ΔT for different sequences where nearly constant ΔT can be achieved after a particular *D*. Thus, the optimal threshold for each video relies on the video content by considering both ΔBDBR and ΔT. For instance, *D*=50 is a proper value for *Undo_Dancer* and *Poznan_Street*, while *D*=30 is more suitable for *Shark*. In order to deal with different characteristics of video sequences, *D* can be periodically updated based on the analysis of coding information in training frames. This may be a more precise way to determine sequence-dependent *D* of the proposed PBED algorithm for our further investigation.

D. Performance of combined scheme (SEDV+PBED)

Besides, we have incorporated both SEDV-based VSO and PBED into HTM-16.0, and let us call them SEDV+PBED. All the previous research works were specified to the old versions of the reference software HTM for 3D-HEVC. Therefore, the performance comparison of related works is not straightforward for depth intra coding. As a result, we compared the works from Park [30], Gu [27] and Zhang [29] employed in HTM-9.0, HTM-7.0 and HTM-5.1, respectively, for the evaluation of SEDV+PBED, and implemented these

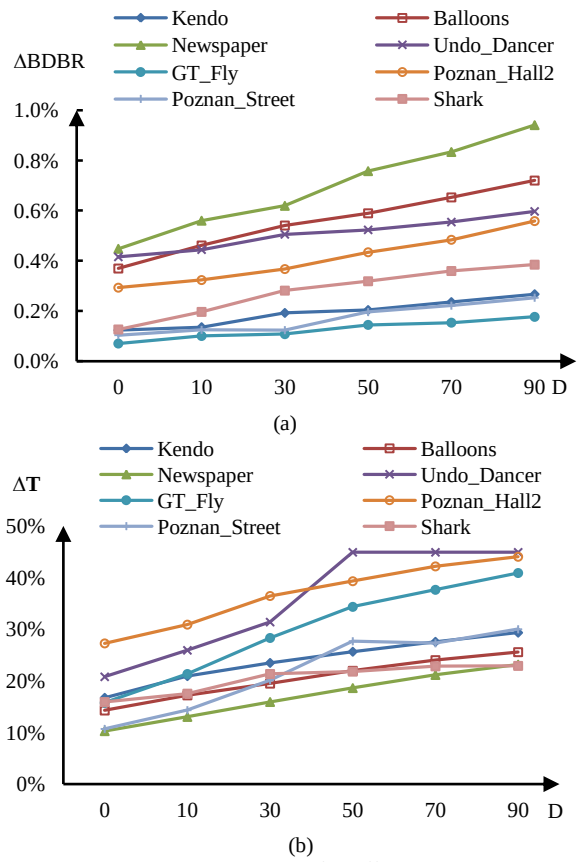

Fig. 12 (a) ΔBDBR and (b) ΔT against *D* for different sequences at QP=34.

algorithms in HTM-16.0. Table IX illustrates the simulation results of various algorithms in terms of ΔBDBR and ΔT. It can be found that both of these algorithms can provide time reduction for depth intra coding. However, the proposed SEDV+PBED reduces about 39% complexity on average and the time savings are only 6%, 10% and 12% in the Park's, Gu's and Zhang's algorithms, respectively. It is due to the fact that PBED can skip both of conventional intra modes and DMM1 in PUs with small $LCRD_{mincost}$. In addition, the simple SEDV-based VSO metric is able to speed up the decision of the optimal wedgelet pattern for the remaining PUs where DMM1 is still used. Actually, the Park's algorithm [30] skips DMM1 for some PUs, which have horizontal or vertical edges, and the variance of which are greater than a threshold. The Gu's algorithm [27] also makes use of LCRD to skip DMM1, but the high complexity caused by the conventional intra mode is still required. The Zhang's algorithm [29] uses the depth level of quadtree to skip DMM1. Since the quadtree is not a good feature for DMM1, this algorithm may skip DMM1 unexpectedly and deteriorate the quality of synthesized views. Besides, there is an overlap between all these algorithms [27], [29]-[30] and [26] in HTM-16.0 for complexity reduction in DMM1. This is another reason for getting only a little time saving by these algorithms. The Park's algorithm employs an edge classification for all sizes of PUs in Hadamard transform domain. In contrast, SEDV+PBED uses the $LCRD_{cost}$ from rough mode decision and only requires a simple arithmetic and comparison operations, without introducing additional

TABLE IX
SIMULATION RESULTS OF STATE-OF-THE-ART ALGORITHMS AND PROPOSED SEDV+PBED

Test sequence	Park's [30]		Gu's [27]		Zhang's [29]		SEDV+ PBED	
	ΔBDBR(%)	ΔT(%)	ΔBDBR(%)	ΔT(%)	ΔBDBR(%)	ΔT(%)	ΔBDBR(%)	ΔT(%)
Kendo	0.13	-11.57	0.63	-8.78	0.97	-9.02	0.43	-38.23
Balloons	0.22	-9.19	1.01	-9.62	1.28	-14.12	0.67	-35.49
Newspaper1	0.24	-5.45	1.50	-11.52	1.31	-10.61	0.89	-33.85
1024x768	**0.19**	**-8.74**	**1.07**	**-9.97**	**1.19**	**-11.25**	**0.66**	**-35.86**
Undo_Dancer	0.18	-6.65	0.62	-8.24	0.94	-15.32	0.49	-41.57
GT_Fly	0.08	-7.84	0.50	-10.51	0.51	-10.16	0.21	-43.14
Poznan_Hall2	0.52	-17.13	0.71	-12.83	1.46	-16.55	0.75	-48.33
Poznan_Street	0.00	5.31	0.74	-9.15	0.79	-10.94	0.29	-39.67
Shark	0.00	2.85	0.89	-9.35	0.85	-10.04	0.33	-34.16
1920x1088	**0.16**	**-4.70**	**0.69**	**-10.02**	**0.91**	**-12.60**	**0.43**	**-41.38**
Avg.	**0.17**	**-6.21**	**0.83**	**-10.00**	**1.01**	**-12.09**	**0.53**	**-39.31**

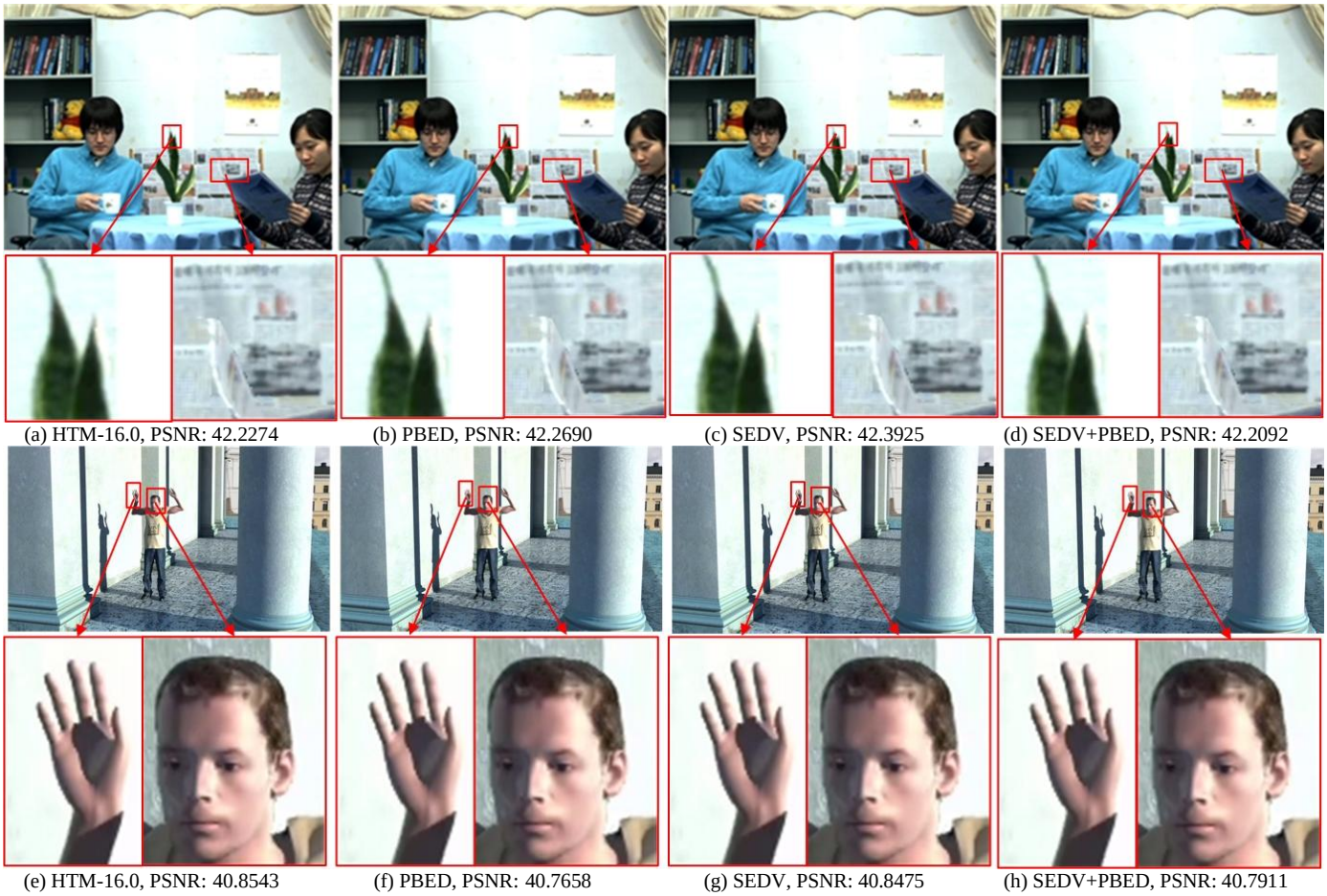

(a) HTM-16.0, PSNR: 42.2274 (b) PBED, PSNR: 42.2690 (c) SEDV, PSNR: 42.3925 (d) SEDV+PBED, PSNR: 42.2092

(e) HTM-16.0, PSNR: 40.8543 (f) PBED, PSNR: 40.7658 (g) SEDV, PSNR: 40.8475 (h) SEDV+PBED, PSNR: 40.7911

Fig. 13. Subjective quality comparison of synthesized views generated by (a) original HTM-16.0 for *Newspaper*, (b) PBED for *Newspaper* , (c) SEDV for *Newspaper*, (d) SEDV+PBED for *Newspaper*, (e) original HTM-16.0 for *Undo_Dancer*, (f) PBED for *Undo_Dancer*, (g) SEDV for *Undo_Dancer*, and (h) SEDV+PBED for *Undo_Dancer*.

overhead such as edge detection. Since the extra computations are introduced in the Park's algorithm, the sequences, *Poznan_Street* and *Shark*, even use more time than HTM-16.0. From Table IX, both of these algorithms make BDBR increasing for all sequences. Compared with these algorithms, a similar BD performance can be achieved by the proposed SEDV+PBED. In addition, Fig. 13 shows the subjective quality comparison of the synthesized views for *Newspaper* and *Undo_Dancer* sequences. It can be seen that the decoded synthesized views of the proposed SEDV, PBED and SEDV+PBED are similar to those of the original HTM-16.0. Fig. 13 also display two zoomed regions for each synthesized views for comparison. From these zoomed regions, it can be seen that the edges in synthesized views generated by the proposed SEDV, PBED and SEDV+PBED can keep the similar quality in comparison to those generated by the original HTM-16.0.

Since the proposed PBED technique also skips DMM1 for some PUs with low rough cost and the proposed SEDV-based VSO metric only focuses on reducing the complexity of DMM1, the percentage of PUs for skipped DMM1 in HTM-16.0 and PBED can be used to verify the compatibility of the two

proposed PBED and SEDV techniques. The technique [26] adopted in HTM-16.0 can skip DMM1 for about 34%, 40%, 57% and 64% PUs at different QPs, as shown in Table VI. In our proposed PBED, the percentages of PUs skipped DMM1 can be improved to about 59%, 63%, 76% and 83% at different QPs. In other words, after integrating PBED into HTM-16.0, about 41%, 37%, 24% and 17% PUs still employ DMM1, which can also be benefit from SEDV-based VSO metric for complexity saving. In addition, a larger PU, in general, contains more complicated texture information and has a large $LCRD_{mincost}$. This case cannot be handled by PBED. Therefore, after the decision of PBED, most of the remaining PUs are large size and have a very huge number of wedgelet patterns as shown in Table I. Notwithstanding, the proposed SEDV-based VSO metric can reduce the extensive computational requirement due to wedgelet pattern decision. Hence, SEDV is a good supplement to the proposed PBED and their integration can achieve a significant time reduction.

VI. Conclusion and Further Work

In this paper, we made a very detailed analysis on the computational requirement of depth intra mode decision. Then, two fast algorithms (PBED and SEDV) have been proposed aiming to speeding up the most time-consuming processes in depth intra mode decision of 3D-HEVC. Based on the statistics of low-complexity rough cost, the time-consuming VSO is entirely skipped and only SDC of one candidate need to be checked by VSO. We then analyzed the relationship between a new metric – SEDV and the optimal wedgelet pattern. By taking this relationship into account, we have suggested a fast DMM1 decision algorithm , which only calculates a very simple but efficient SEDV instead of the complicated VSO metric to select the optimal wedgelet pattern candidate. Simulation results clearly showed that the new scheme with the two proposed techniques provides up to 33%-48% time reduction for depth coding, while keeping the comparable BD performance.

In the future, some effective and efficient ways to determine the optimal threshold in PBED will be studied. As mentioned in Section IV-B and Section V-C, it depends on the conditional probability and the characteristics of video sequences. They can also be estimated by the probability-based model, such as the Bayesian classifier, Markov Network, and Random forest. It may then include on-line training or update process for the threshold optimization. It is also interesting to note that the proposed algorithms in this paper are mainly based on the empirical observation, which is very common approach in the development of depth intra mode decision [30], [42], and texture intra mode decision [48], [52]-[54]. Although this is reasonable approach, another challenging research topic is to formulate an analytical model that can be applied to a wider range of video scenarios for depth intra mode decision. These could be a point of our immediate future works.

References

[1] O. Schreer, I. Feldmann, N. Atzpadin, P. Eisert, P. Kau, and H. J. W. Belt, "3D presence -A system concept for multi-user and multi-party immersive 3D video conferencing," in *Proc. European Conf. Vis. Media Produ. (CVMP)*, Nov. 2008, pp. 1-8.

[2] Microsoft Company, [Online] Available: http://www.xbox.com/

[3] A. Vetro, T. Wiegand, and G. J. Sullivan, "Overview of the Stereo and multi-view video coding extensions of the H.264/MPEG-4 AVC standard," *Proc. of IEEE*, vol. 99, no 4, pp. 626-642, Apr. 2011.

[4] Y. Chen, M. M. Hannuksela, T. Suzuki, and S. Hattori, "Overview of the MVC+D 3D video coding standard," *J. Vis. Commun. Image Represent.*, vol. 25, no. 4, pp. 679-688, May 2014.

[5] A. Smolic *et al*., *Multi-view video plus depth (MVD) format for advanced 3D video systems*, document JVT-W100, Joint Collaborative Team on 3D Video Coding Extension Development (JCT-3V) of ITU-T SG 16 WP 3 and ISO/IEC JTC 1/SC 29/WG 11, San Jose, Apr. 2007.

[6] *Call for proposals on 3D video coding technology*, document N12036, Motion Picture Expert Group (MPEG), Mar. 2011.

[7] K. Muller, P. Merkle, and T. Wiegand, "3D video representation using depth maps," *Proc. of IEEE Special Issue 3D Media Displays*, vol. 99, no. 4, pp. 643-656, Apr. 2011.

[8] P. Kau, N. Atzpadin, C. Fehn, M. Muller, O. Schreer, A. Smolic, and R. Tanger, "Depth map creation and image based rendering for advanced 3DTV services providing interoperability and scalability," *Signal Process. Image Commun. Special Issue 3DTV*, vol. 22, no. 2, pp. 217-234, Feb. 2007.

[9] G. J. Sullivan, J.-R. Ohm, W.-J. Han, and T. Wiegand, "Overview of the high efficiency video coding (HEVC) standard," *IEEE Trans. Circuits Syst. Video Technol.*, vol. 22, no. 12, pp. 1649-1668, Dec. 2012.

[10] K. Muller *et al.* "3D High-efficiency video coding for multi-view video and depth data," *IEEE Trans. Image Process.*, vol. 22, no. 9, pp. 3366-3378, Sep. 2013.

[11] P. Merkle, Y. Morvan, A. Smolic, D. Farin, K. Muller, P. H. N. de With, and T. Wiegand, "The effects of multiview depth video compression on multiview rendering," *Signal Process., Image Commun*., vol. 24, no. 1-2, pp. 73-88, Jan. 2009.

[12] K. Muller, P. Merkle, G. Tech, and T. Wiegand, "3D video coding with depth modeling modes and view synthesis optimization," in *Proc. IEEE Int. Conf. APSIPA ASC*, Dec. 2012, pp. 1-4.

[13] F. Jager, "Simplified depth map intra coding with an optional depth lookup table", in *Proc. Int. Conf. 3D Imaging*, Dec. 2012, pp. 1-4.

[14] P. Merkle, K. Muller, and T. Wiegand, "Coding of depth signals for 3D video using wedgelet block segmentation with residual adaptation," in *Proc. Int. Conf. Multimedia and Expo (ICME)*, Jul. 2013, pp. 1-6.

[15] I. Daribo, G. Cheung, and D. Florencio, "Arithmetic edge coding for arbitrarily shaped sub-block motion prediction in depth video compression", in *Proc. Int. Conf. Image Process. (ICIP)*, Stp./Oct., 2012, pp. 1541-1544.

[16] C.-H. Fu, H.-B. Zhang, W.-M. Su, S.-H Tsang and Y.-L. Chan, "Fast wedgelet pattern decision for DMM in 3D-HEVC," *in Proc. IEEE Int. Conf. Digital Signal Processing (DSP)*, Jul. 2015, pp.477-481.

[17] H.-B. Zhang, C.-H. Fu, Y.-L. Chan, S.-H. Tsang, W.-C. Siu and W.-M. Su, "Efficient wedgelet pattern decision for depth modeling modes in three-dimensional high-efficiency video coding," *J. Electron. Imaging*, vol. 25, no.3, May/Jun. 2016.

[18] W.-J. Han *et al*., "Improved video compression efficiency through flexible unit representation and corresponding extension of coding tools," *IEEE Trans. Circuits Syst. Video Technol.*, vol. 20, no. 12, pp. 1709–1720, Dec. 2010.

[19] G. Tech *et al*. "3D video coding using the synthesized view distortion change," in *Proc. Picture Coding Symposium* (PCS), May 2012, pp. 25-28.

[20] B. T. Oh, J. Lee, and D. Park, "Depth map coding based on synthesized view distortion function," *J. Sel. Topics Signal Process.*, vol. 5, no.7, pp. 1344-1352, Oct. 2011.

[21] J. Lainema, F. Bossen, W.-J. Han, J. Min, and K. Ugur, "Intra coding of the HEVC standard," *IEEE Trans. Circuits Syst. Video Technol.*, vol.22, no.12, pp.1792-1801, Dec. 2012.

[22] Y. Chen, G. Tech, K. Wegner, and S. Yea, *Test Model 11 of 3D-HEVC and MV-HEVC*, document JCT3V-K1003, Joint Collaborative Team on 3D Video Coding Extension Development (JCT-3V) of ITU-T SG 16 WP 3 and ISO/IEC JTC 1/SC 29/WG 11, 11th Meeting, Geneva, CH, 12–18 Feb. 2015.

[23] J. Y. Lee, M. W. Park, Y. J. Cho, and C. Y. Kim, *3D-CE2 related: Separate enabling flag for intra coding tools*, document JCT3V-I0085, Joint Collaborative Team on 3D Video Coding Extension Development (JCT-3V) of ITU-T SG 16 WP 3 and ISO/IEC JTC 1/SC 29/WG 11, 9th Meeting, Sapporo, JP, 3–9, Jul. 2014.

[24] L. Zhao, L. Zhang, S. Ma, and D. Zhao, "Fast Mode Decision Algorithm for Intra Prediction in HEVC," in *Proc. IEEE Int. Conf. Vis. Commu. and Image Process. (VCIP)*, Nov. 2011, pp. 1- 4

[25] D. Marpe *et al.* "Video compression using nested quadtree structures, leaf merging, and improved techniques for motion representation and entropy coding," *IEEE Trans. Circuits Syst. Video Technol.*, vol. 20, no. 12, pp. 1676– 1687, Dec. 2010.

[26] Z. Y. Gu, J. H. Zheng, N. Ling, and P. Zhang, "Fast Depth Modeling Mode Selection for 3D HEVC Depth Intra Coding", in *Proc. IEEE Int. Conf. Mulimedian and Expo Workshop (ICMEW)*, Jul. 2013, pp. 1-4.

[27] Z. Y. Gu, J. H. Zheng, L. Nam, and P. Zhang , "Fast bi-partition mode selection for 3D HEVC depth intra coding," in *Proc. IEEE Int. Conf. Mulimedian and Expo (ICME)*, Jul. 2014, pp. 1-6.

[28] T. D. Silva, L. Agostini, and L. D. S. Cruz, "Complexity reduction of depth intra coding for 3D video extension of HEVC," in *Proc. IEEE Int. Conf. Vis. Commu. and Image Process. (VCIP)*, Dec. 2014, pp. 229-232.

[29] Q. W. Zhang, N. N. LI, L. X. Xun and Y. Gan, "Effective early terminate algorithm for depth map intra coding in 3D-HEVC," *Electron. Lett.*, vol. 50, no. 14, Jul. 2014, pp. 994-996.

[30] C. S. Park, "Edge-Based intra mode selection for depth-map coding in 3D-HEVC," *IEEE Trans. Image Process.*, vol. 24, no. 1, Jan. 2015.

[31] G. Sanchez, M. Saldanha, G. Balota, B. Zatt, M. Porto, and L. Agostini, "Complexity reduction for 3D-HEVC depth maps intra-frame prediction using simplified edge detector algorithm," in *Proc. IEEE Int. Conf. Image Process. (ICIP)*, Oct. 2014, pp. 3209-3213.

[32] P. Merkle, K. Müller, X. Zhao, Y. Chen, and L. Zhang, *Simplified Wedgelet search for DMM modes 1 and 3*, Joint Collaborative Team on 3D Video Coding Extension Development (JCT-3V) of ITU-T SG 16WP 3 and ISO/IEC JTC 1/SC 29/WG 11, document JCT3V-B0039, Shanghai, China, Oct. 2012.

[33] M. M. Zhang, C. Zhao, J. Z. Xu, and H. H. Bai, "A fast depth-map wedgelet partitioning scheme for intra prediction in 3D video coding," in *Proc. IEEE Int. Sympo. Circuits and Syst. (ISCAS)*, May 2013, pp. 2852-2855.

[34] G. Sanchez, M. Saldanha, G. Balota, B. Zatt, M. Porto, and L. Agostini, "A complexity reduction algorithm for depth maps intra prediction on the 3D-HEVC," in *IEEE Int. Conf. Vis. Commu. and Image Process. (VCIP)*, Dec. 2014, pp. 137-140.

[35] L. F. R. Lucas, K. Wegner, N. M. M. Rodrigues, C. L. Pagliari, E. A. B. Silva and S. M. M. Faria, "Intra Predictive Depth Map Coding Using Flexible Block Partitioning," *IEEE Trans. Image Process.*, vol. 24, no. 11, Nov. 2015, pp. 4055-4068.

[36] C. Y. Li, X. J, and Q. H. Dai, "A novel distortion model for depth coding in 3D-HEVC," in *Proc. IEEE Int. Conf. Image Process. (ICIP)*, Oct. 2014, pp. 3228 – 3232.

[37] T. O. Byung and J. O. Kwan, "View Synthesis Distortion Estimation for AVC- and HEVC-Compatible 3-D Video Coding," *IEEE Trans. Circuits Syst. Video Technol.*, vol. 24, no. 6, pp.1006-1015, Jun. 2014.

[38] Z. Y. Gu, J. H. Zheng, and N. Ling, *Fast intra SDC coding for 3D-HEVC intra coding*, Joint Collaborative Team on 3D Video Coding Extension Development (JCT-3V) of ITU-T SG 16 WP 3 and ISO/IEC JTC 1/SC 29/WG 11, document JCT3V-I0123, 9th Meeting, Sapporo JP, July 2014.

[39] J. Y. Lee, M. W. Park, and Y. Jin, *3D-CE2 related: Fast SDC DC offset decision*, Joint Collaborative Team on 3D Video Coding Extension Development (JCT-3V) of ITU-T SG 16 WP 3 and ISO/IEC JTC 1/SC 29/WG 11, document JCT3V-I0084, 9th Meeting, Sapporo JP, Jul. 2014.

[40] E. G. Mora, J. Jung, M. Cagnazzo, and B. Pesquet, "Initialization, limitation, and predictive coding of the depth and texture quadtree in 3D-HEVC," *IEEE Trans. Circuits Syst. Video Technol.*, vol. 24, no.9, pp. 1554-1565, Sept. 2014.

[41] C. S. Park. "Efficient intra-mode decision algorithm skipping unnecessary depth modelling modes in 3D-HEVC," *Electron. Lett.*, vol. 51, no. 10, 2015, pp. 756-758.

[42] Q. W. Zhang, Y. S. Yang, H. W. Chang, W. W. Zhang, and Y. Gan, "Fast intra mode decision for depth coding in 3D-HEVC." *Multidimensional Syst. and Signal Process.*, Online Early Access, 2016, pp. 1-24.

[43] Y. H. Zhang, C. Zhu, Y. B. Lin, J. H. Zheng, and Y. Wang, "An Efficient Partition Scheme for Depth-Based Block Partitioning in 3D-HEVC," in *Proc. Advances in Multimedia Informa. Process Pacific-Rim Conf. Multimedia. (PCM)*, Sep. 2015, pp. 428-436.

[44] X. G. Zhang, K. Zhang, J. C. An, J. L. Lin, and S. M. Lei, *3D-CE2 related: A texture-partition-dependent depth partition for 3D-HEVC*, ITU-T SG 16 WP 3 and ISO/IEC JTC 1/SC 29/WG 11, document JCT3V-G0055, 7th Meeting, San Jose, US, 11–17, Jan. 2014.

[45] H. Brust, K. Muller, and T. Wiegand, *3D-CE6.h related: Results on modified depth coding in random access units*, Joint Collaborative Team on 3D Video Coding Extension Development (JCT-3V) of ITU-T SG 16 WP 3 and ISO/IEC JTC 1/SC 29/WG 11, document JCT3V-C0160, 3rd Meeting, Geneva, CH, 17-23, Jan. 2013.

[46] S. Cho, and M. Kim, "Fast CU splitting and pruning for suboptimal CU partitioning in HEVC intra coding," *IEEE Trans. Circuits Syst. Video Technol.*, vol.23, no.9, pp.1555-1564, Sep. 2013

[47] H. Q. Zeng, K.-K Ma and C. Cai, "Hierarchical Intra Mode Decision for H.264/AVC," *IEEE Trans. Circuits Syst. Video Technol.*, vol. 20, no. 6, pp. 907-912, Jun. 2010.

[48] L. Shen, Z. Zhang and Z. Liu, "Effective CU Size Decision for HEVC Intracoding," *IEEE Trans. Image Process.*, vol. 23, no. 10, pp. 4232-4241, Oct. 2014.

[49] F. Bossen *et al.*, *3D-HEVC software HTM-16.0*. [Online]. Available: https://hevc.hhi.fraunhofer.de/svn/svn 3DVCSoftware /tags/HTM-16.0, Oct. 2015.

[50] K. Muller, and A. Vetro, *Common test conditions of 3DV core experiments*, Joint Collaborative Team on 3D Video Coding Extension Development (JCT-3V) of ITU-T VCEG and ISO/IEC MPEG, document JCT3V-G1100, Jan. 2014.

[51] G. Bjontegaard, "Calculation of Average PSNR Differences between RD Curves," ITU-T Video Coding Experts Group (VCEG), 2001: ITU-T SG 16 Q.6 Document, VCEG-M33, Austin, Apr. 2001.

[52] W. Zhao, T. Onoye and T. Song, "Hierarchical Structure-Based Fast Mode Decision for H.265/HEVC," *IEEE Trans. Circuits Syst. Video Technol.*, vol. 25, no. 10, pp. 1651-1664, Oct. 2015.

[53] L. Shen, Z. Zhang and P. An, "Fast CU size decision and mode decision algorithm for HEVC intra coding," *IEEE Trans. Consumer Electron.*, vol. 59, no. 1, pp. 207-213, Feb. 2013.

[54] K. Lim, J. Lee, S. Kim and S. Lee, "Fast PU Skip and Split Termination Algorithm for HEVC Intra Prediction," *IEEE Trans. Circuits Syst. Video Technol.*, vol. 25, no. 8, pp. 1335-1346, Aug. 2015.